Adsorption, Diffusion, and Dissociation of H_2S on Fe(100) from First Principles

D. E. Jiang and Emily A. Carter*

Department of Chemistry & Biochemistry, Box 951569, University of California, Los Angeles, California 90095-1569

Received: August 5, 2004; In Final Form: October 4, 2004

We employ spin-polarized periodic density functional theory (DFT) to characterize H_2S and HS adsorption, diffusion, and dissociation on the Fe(100) surface. We investigate the site preference of H_2S, HS, and S on Fe(100). H_2S is predicted to weakly adsorb on hollow, bridge, and on-top sites of Fe(100), with the bridge site preferred. The diffusion barrier from the bridge site to the next most stable on-top site is predicted to be small (∼0.15 eV). In contrast to H_2S, HS is predicted to be strongly chemisorbed on Fe(100), with the S atom in the hollow site and the HS bond oriented perpendicular to the surface, due to charge transfer from the surface to S p-orbitals. Isolated S atoms also are predicted to bind strongly to the hollow sites of Fe(100), with the bridge site found to be a transition state for S hopping between neighboring hollow sites. The minimum energy paths for H_2S and HS dehydrogenation involve rotating an H atom toward a nearby surface Fe atom, with the S−H bonds breaking on the top of only one Fe atom. The barriers to break the first and second S−H bonds in H_2S are low and about the same, ∼0.25 eV, suggesting deposition of S on Fe(100) via H_2S is kinetically and thermodynamically facile, consistent with experiments.

Introduction

Gases containing hydrogen sulfide (H_2S) attack structural metals such as iron aggressively. Sulfur forms stable sulfides with many transition metals,[1] including Fe. Due to the largely favorable thermodynamics and the relatively weak H−S bond, the barriers for H_2S dissociation on transition metal surfaces are usually very small.[2−4] This leads to a fast sulfur deposition on metal surfaces and subsequent sulfide formation. For example, FeS formation is observed in many eroded steel gun tubes, where H_2S is produced after gun firing from precursors such as S-containing flash suppressants, primers, and igniters that are added to propellants.[5] Sulfur can also cause the embrittlement of transition metals such as Ni and Fe.[6] Moreover, because H_2S deposits its hydrogen atoms on transition metal surfaces, those hydrogen atoms can also embrittle metals such as Fe.[7,8] Here, our objective is to characterize how H_2S dissociates on iron surfaces, with the eventual goal of suggesting ways to prevent sulfide formation or hydrogen embrittlement of steel.

Most experimental studies of H_2S interaction with iron have employed polycrystalline iron films.[9−12] Using X-ray photoelectron spectroscopy (XPS), Narayan et al. studied iron sulfidation by H_2S from 100 to 773 K.[9] On the basis of binding energy shifts of the S 2p level, they concluded that H_2S adsorption is molecular at 100 K, but dissociative from 190 K up to ambient temperatures. At $T > 423$ K, they found formation of FeS, where the initial nonstoichiometric form converts to the stoichiometric form with increased H_2S dosing. No direct evidence [such as high-resolution electron energy loss spectroscopy (HREELS)] was presented to confirm the molecular adsorption of H_2S at 100 K. Most other H_2S adsorption experiments on iron surfaces were performed at room temperature or above, where no molecular H_2S or HS was observed, indicating the ease of H_2S dissociation.

* Corresponding author. Phone: +1-310-206-5118. Fax: +1-310-267-0319. E-mail: eac@chem.ucla.edu.

In this work, we characterize the H_2S and HS adsorption sites, diffusion barriers, and dissociation pathways on Fe(100) with periodic density functional theory (DFT).

Calculational Details

We perform first-principles calculations based on spin-polarized density functional theory (DFT).[13,14] The Vienna Ab Initio Simulation Package (VASP)[15,16] is used to solve the Kohn−Sham equations with periodic boundary conditions and a plane-wave basis set. Here, we employ Blöchl's all-electron (with frozen core) projector augmented wave (PAW) method[17] as implemented by Kresse and Joubert.[18] We use the generalized gradient approximation (GGA) of PBE for the treatment of electron exchange and correlation.[19]

We use a kinetic energy cutoff of 400 eV for all of the calculations, which converges the total energy to ∼1 meV/atom for the primitive cell of bulk Fe. The Monkhorst−Pack scheme[20] is used for the k-point sampling. The first-order Methfessel−Paxton method[21] is used for the Fermi surface smearing, with a width of 0.1 eV to obtain accurate forces. An equilibrium lattice constant of 2.83 Å is used for ferromagnetic bcc Fe, as we obtained earlier with a converged k-mesh of 15 × 15 × 15.[22] This lattice constant agrees well with the experimental value of 2.86 Å.[23]

To model gaseous H_2S, HS, and S atom, we place a molecule or atom in a 10 Å cubic box. We perform a non-spin-polarized calculation for H_2S, but spin-polarized calculations for open-shell HS and S, where the valence electron configuration used for S atom is triplet $(3p)^4$, approximately the ^3P ground state (spin-polarized DFT "wave functions" are slightly spin-contaminated). Tables 1 and 2 display the molecular geometry, vibrational frequencies, and bond dissociation energies from our work, which are in good agreement with experiment.

Table 3 shows the interlayer relaxation for clean Fe(100) from the present work and other theoretical work, as compared to low-energy electron diffraction (LEED) measurements. One can

10.1021/jp046475k CCC: $27.50
Published on Web 11/19/2004

TABLE 1: PAW-GGA(PBE) Results for Gaseous H_2S: Asymmetric Stretching Frequency (ω_a), Symmetric Stretching Frequency (ω_s), Bending Frequency (ω_b), Equilibrium Bond Length ($R_{S-H,e}$), H−S−H Bond Angle (θ_{H-S-H}), and HS−H Bond Dissociation Energy [D_e(HS−H)]

method	ω_a (cm^{-1})	ω_s (cm^{-1})	ω_b (cm^{-1})	$R_{S-H,e}$ (Å)	θ_{H-S-H} (deg)	D_e(HS−H) (eV)
PAW-GGA	2618	2607	1151	1.349	91.6	4.19
exp.[a]	2628	2615	1183	1.328	92.2	4.14

[a] Frequencies, bond lengths, and bond angles are from ref 36; the experimental D_e(HS−H) is obtained by performing a zero-point-energy correction (with experimental H_2S and HS vibrational frequencies cited in Tables 1 and 2) to the measured D_0(HS−H) from ref 37.

TABLE 2: PAW-GGA(PBE) Results for Gaseous HS: Stretching Frequency (ω_s), Equilibrium Bond Length ($R_{S-H,e}$), and HS Equilibrium Dissociation Energy (D_e)

HS	ω_s (cm^{-1})	$R_{S-H,e}$ (Å)	D_e (eV)
PAW-GGA	2616	1.354	3.70
exp.[a]	2660	1.345	3.78

[a] Reference 38. The experimental D_e was extracted in the same manner as described in Table 1, footnote a.

TABLE 3: Percentage of Interlayer Relaxation ($\Delta_{i,i+1}$)[a] for Fe(100)

method	# of layers	Δ_{12}	Δ_{23}
PAW-GGA(PBE)[b]	5	−2.2	4.3
	7	−2.9	3.0
USPP-GGA(PW91)[c]	5	−4.3	3.1
	7	−3.8	2.7
USPP-GGA(PW91)[d]	5	−3.5	2.3
FLAPW-GGA(PBE)[e]	5	−4	1.5
experiment[f]		−5 ± 2	5 ± 2

[a] $\Delta_{i,i+1}$ is defined as the percentage change of interlayer spacing between substrate layer i and $i+1$, as compared to the bulk spacing d_0. Layer 1 is the topmost substrate layer. [b] Present work. [c] Reference 39. [d] Reference 40. [e] Reference 41. [f] From low-energy electron diffraction.[42]

see that theoretical results vary with the number layers in the slab and are different from one study to another, but they all show the same trends that agree qualitatively with experiment: contraction of the surface layer toward bulk with concomitant expansion of the next interlayer spacing.

We chose a five-layer slab to model Fe(100) and put adsorbates on one side of the slab; this produces a small dipole due to the dipole of the molecular adsorbate itself and to charge transfer between the adsorbate and the metal surface. However, we did not bother with a dipole correction to the total energy because it was generally small (<0.03 eV/cell). Only the top two layers of the five substrate layers are allowed to relax, together with the adsorbate layer. The bottom three layers are kept fixed in bulk positions to represent the semi-infinite bulk crystal beneath the surface. (Allowing the middle layer of the substrate to relax only changes the total energy of the slab by ∼5 meV.) When the maximum force acting on each of the relaxed atoms drops below 0.01 eV/Å, the structural relaxation is stopped.

In this work, we study the 0.25 ML coverage only. Experiments show that 0.50 ML coverage can be easily achieved for S on Fe(100) as a $c(2\times2)$ superstructure. However, no direct observations of H_2S or HS on Fe(100) are available. We chose 0.25 ML as a compromise between minimizing adsorbate−adsorbate interactions and being close to the coverage of the stable overlayer structure of S on Fe(100) from experiment. Future work may involve coverage effects on adsorption, diffusion, and dissociation of H_2S on Fe(100). High-symmetry sites on Fe(100) are displayed in Figure 1. We use a k-mesh of $4 \times 4 \times 1$ for the $p(2\times2)$ Fe(100) cell, which converges the adsorption energy of H_2S to within 0.02 eV.

The Climbing Image Nudged Elastic Band (CI-NEB) method[24,25] is used to locate the minimum energy paths (MEPs)

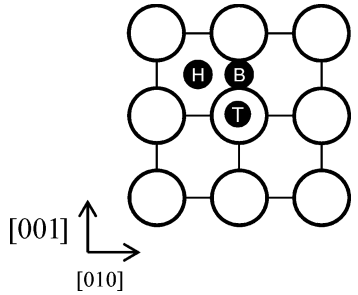

Figure 1. High-symmetry adsorption sites on Fe(100): on-top (T) site, two-fold bridge (B), and four-fold hollow (H).

and the transition states for H_2S and H diffusion, as well as for H_2S and HS dissociation on Fe(100). An interpolated chain of configurations (images) between the initial and final positions are connected by springs and relaxed simultaneously to the MEP. With the climbing image scheme, the highest-energy image climbs uphill to the saddle point. We use the same force tolerance for the transition state search as that for structural relaxations. Typically, we first use the normal NEB method for ∼10 iterations (ionic steps) to roughly converge the MEP, and then switch on the climbing-image algorithm. After ∼50 more iterations, we can converge both the MEP and the TS to the preset force tolerance.

Vibrational frequencies of H_2S and HS on Fe(100) are determined by diagonalizing a finite difference construction of the Hessian matrix with displacements of 0.02 Å (only allowing H and S atoms to move). The natures of the relaxed adsorbate configurations and the saddle points found by the CI-NEB method are also verified via the same type of vibrational frequency calculations.

Results and Discussion

1. H_2S Adsorption on Fe(100). Two experimental studies of H_2S interactions with Fe(100) have been reported previously, using low-energy electron diffraction (LEED) and Auger electron spectroscopy (AES).[26,27] However, no adsorption geometry of molecular H_2S on Fe(100) was inferred from that work. The structures of three predicted local minima for molecular adsorption are shown in Figure 2. The corresponding predicted adsorption energies, geometries, and vibrational frequencies are given in Table 4. H_2S is predicted to be quite weakly adsorbed, favoring the bridge site with an adsorption energy of −0.46 eV, followed by the on-top site (−0.33 eV) and the hollow site (−0.13 eV).

Given this fairly weak interaction, we decided to also use the RPBE exchange-correlation functional[28] for H_2S adsorption on Fe(100), with PBE-optimized geometries. As usual, DFT-RPBE reduces the typical overbinding between adsorbates and the metal surface by DFT-PBE. The resulting adsorption energies are only slightly negative (∼ −0.05 eV) and are very similar for the bridge and the on-top sites, indicating the interaction between H_2S and Fe(100) is exceedingly weak, while the adsorption at the hollow site is predicted to be energetically

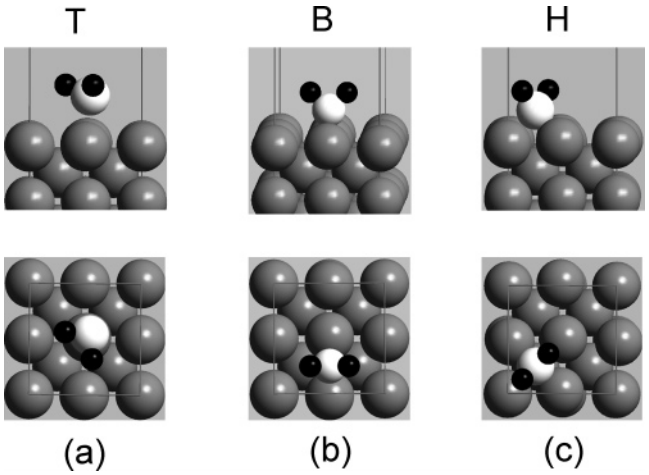

Figure 2. The high-symmetry adsorption sites of H_2S on Fe(100): (a) on-top; (b) bridge; (c) hollow. The upper panel is the side view, and the lower panel is the top view. Fe atoms are in gray, S atoms are in white, and H atoms are in black.

TABLE 4: Adsorption Energy [$E_{ad} = E(H_2S/Fe\text{-slab}) - E(Fe\text{-slab}) - E(H_2S)$] of H_2S on Fe(100), H−S Bond Length ($R_{S-H,e}$), H−S−H Bond Angle (θ_{HSH}), and Asymmetric Stretching Frequency (ω_a), Symmetric Stretching Frequency (ω_s), and Bending Frequency (ω_b) of H_2S at $\theta = 0.25$ ML

	bridge	on-top	hollow
E_{ad} (eV)	−0.46	−0.33	−0.13
$R_{S-H,e}$ (Å)	1.373	1.362	1.399
θ_{HSH} (deg)	91.7	91.0	86.5
ω_a (cm^{-1})	2342	2478	2050
ω_s (cm^{-1})	2375	2500	2180
ω_b (cm^{-1})	1164	1149	1179

unfavorable by DFT-RPBE. We caution that such weak interactions are not well described by conventional DFT-GGA theory and that functionals capable of describing van der Waals interactions are at the frontiers of DFT.[29]

While the geometry of H_2S (Table 4) changes only slightly upon adsorption (a slight lengthening of the S−H bonds; see Table 1), the asymmetric and symmetric stretching frequencies of H_2S are softened noticeably upon adsorption. Interestingly, the bending frequency is essentially unchanged upon adsorption.

The orientation of H_2S in the bridge site is strongly suggestive of Fe−S dative bonding via S lone electron pairs, which are localized in the plane perpendicular to the H−S−H plane. We predict a diffusion barrier for H_2S moving from the bridge site to the on-top site of ∼0.15 eV, indicating the mobility of H_2S on Fe(100) is high. This barrier is only slightly larger than the stability difference (0.13 eV) between the bridge and on-top sites. We therefore estimate that the diffusion barrier for H_2S moving from the on-top site to the hollow site will be close to the thermodynamic energy difference of ∼0.20 eV.

2. HS Adsorption on Fe(100). Figure 3 shows the three high symmetry adsorption sites considered for HS on Fe(100), and Table 5 displays their corresponding energetics, vibrational frequencies, and geometries. Only the hollow site is a local minimum, with the HS bond pointing along the surface normal and an H−S vibrational frequency of 2197 cm^{-1}, which is ∼400 cm^{-1} smaller than the gaseous value. Because we ignore coupling to the substrate (i.e., we keep it fixed for vibrational frequency analysis), then in addition to the H−S stretching mode, five other modes exist for HS vibrations on Fe(100): two frustrated rotational and three frustrated translational modes. The two frustrated rotational modes at 463 and 470 cm^{-1} correspond to H−S surface bending motion for HS at the hollow site. The

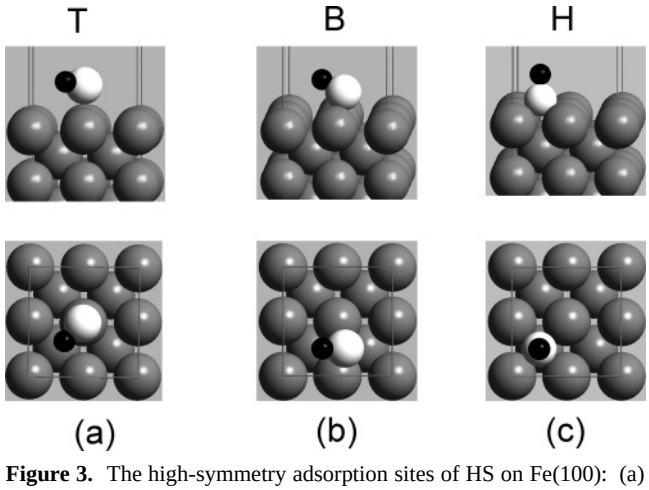

Figure 3. The high-symmetry adsorption sites of HS on Fe(100): (a) on-top; (b) bridge; (c) hollow. The upper panel is the side view, and the lower panel is the top view. Fe atoms are in gray, S atoms are in white, and H atoms are in black.

TABLE 5: Adsorption Energy [$E_{ad} = E_{HS/Fe-slab} - E_{Fe-slab} - E_{HS}$] of HS on Fe(100), H−S Bond Length ($R_{S-H,e}$), Tilt Angle of H−S Bond Axis with Respect to the Surface normal (θ), H−S Stretching Frequency (ω_s), H−S Surface Bending Frequency (ω_b), and HS Surface Frustrated Translation Frequency (ω_t) of HS at $\theta = 0.25$ ML[a]

	on-top	bridge	hollow
E_{ad} (eV)	−2.76 (hos)[b]	−3.30 (ts)[c]	−3.56 (min)
$R_{S-H,e}$ (Å)	1.355	1.363	1.393
θ (deg)	80.5	58.9	0
ω_s (cm^{-1})	2586	2498	2197
ω_b (cm^{-1})	73, 450	448, 510	463, 470
ω_t (cm^{-1})	38i, 53i, 266	17i, 154, 237	182, 190, 204

[a] The nature of the critical point is given in parentheses (min = minimum, ts = transition state, and hos = higher-order saddle point). [b] The two modes with imaginary frequencies correspond to frustrated translational modes. [c] The mode with the imaginary frequency corresponds to a reaction coordinate for HS diffusion between four-fold hollow sites.

three translational modes usually consist of two lateral modes and one adsorbate−substrate stretching mode. However, the lateral modes are strongly coupled with the HS surface stretching mode for HS at the hollow site, yielding similar frequencies at 182, 190, and 204 cm^{-1}. The imaginary frequency modes for HS at the on-top and bridge sites correspond to frustrated translations. In particular, this mode at the bridge site corresponds to a reaction coordinate for HS diffusion between neighboring hollow sites.

Figure 4 displays an electron density difference plot for HS at the hollow site. One can see that electron density is depleted from under the S atom and from the four surface Fe atoms, with electron density accumulating around the S atom. The accumulated electron density appears to be in the S p-orbitals. The symmetrical interaction of those p-orbitals with the four surface Fe atoms may be responsible for the perpendicular orientation of adsorbed HS in the four-fold hollow site. As intimated above, the bridge site is a transition state for HS diffusion on Fe(100) between neighboring hollow sites, with a predicted barrier of 0.26 eV. In contrast, the on-top site is neither a minimum nor a transition state, but is a rank-2 saddle point. Consistent with these predictions, recent low-temperature STM images of HS adsorption on Cu(100) by Lauhon and Ho[30] indicate that HS adsorbs upright on the four-fold hollow site of Cu(100). Although Cu has an fcc lattice and Fe has a bcc lattice, and are thus not directly comparable, Cu(100) and Fe(100) do both have four-fold symmetry. Future STM experiments should

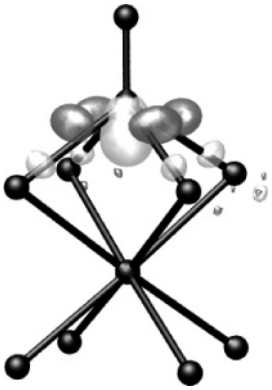

Figure 4. Isosurface plot of the electron density difference, $\Delta\rho$, for HS/Fe(100) in the hollow site. Solid black balls represent atoms: the top one is H, the one below H is S, and the atoms below S are Fe atoms. The iso-value is at -0.05 e/Å^3 for the light gray surface and at 0.05 e/Å^3 for the dark gray surface. Negative $\Delta\rho$ indicates loss of electron density upon binding.

TABLE 6: Adsorption Energy [$E_{ad} = E_{S/Fe-slab} - E_{Fe-slab} - E_S$] of S Atom on Fe(100), the Height of S Atom Above the First Substrate Layer (d), and S Surface Frustrated Translation Frequency (ω_t) at $\theta = 0.25$ ML[a]

	on-top	bridge	hollow
E_{ad} (eV)	−4.06 (hos)	−4.79 (ts)	−6.00 (min)
d (Å)	1.96	1.75	1.03
ω_t (cm^{-1})	93i, 100i, 378	75i, 192, 317	225, 228, 233

[a] The nature of the critical point is given in parentheses (min = minimum, ts = transition state, and hos = higher-order saddle point).

be able to verify whether this prediction of the adsorption site for HS on Fe(100) is correct.

3. S Adsorption on Fe(100). LEED experiments show[31] that sulfur forms a $c(2\times2)$ superstructure on Fe(100) ($\theta_S = 0.5$ ML) and that S atom prefers the hollow site of Fe(100), which has been confirmed by a previous DFT-LDA study.[32] Our DFT-GGA results also indicate that S prefers the hollow site at $\theta_S = 0.25$ ML, with the hollow site as the only minimum (Table 6; the nature of the critical point is again verified by normal-mode analysis). The height of S above the surface is found to be 1.03 Å for the hollow site, in good agreement with the experimental value of 1.09 Å at 0.50 ML.[31] As for HS on Fe(100), the bridge site is a transition state for S diffusion on Fe(100), albeit with a considerably higher barrier of 1.21 eV. As in the case of $HS_{(ad)}$, the on-top site is not a minimum nor a transition state, but is a rank-2 saddle point.

The binding between S and Fe(100) is 2.44 eV stronger than that between HS and Fe(100), which in turn is 3.10 eV stronger than the binding between H_2S and Fe(100), when we compare adsorption in their respective most stable sites. The thermodynamic driving force is therefore large for H_2S dissociation on Fe(100).

Our earlier work[33] shows that both the bridge and the hollow sites are minima for H on Fe(100), while the on-top site is a rank-2 saddle point. We found that adsorption of H into either site is nearly equally favorable (within ~0.06 eV) at 0.25 ML. The barrier for H to diffuse from the hollow site to the bridge site is calculated to be ~0.12 eV, where the transition state has the H atom midway between the bridge site and the hollow site. This will be relevant in our discussion of H_xS ($x = 1, 2$) dissociation, as we now discuss.

4. H_2S Dissociation on Fe(100). As stated earlier, we use the nudged elastic band (NEB) method to locate the minimum energy path for H_2S dissociation to HS and H. The NEB method

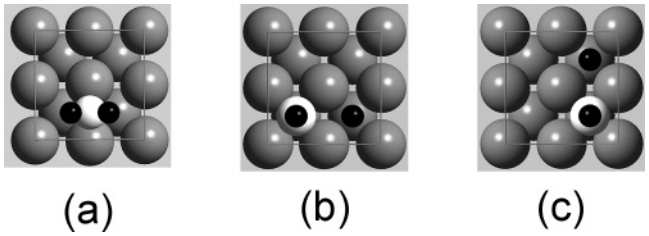

Figure 5. Initial and final states considered for H_2S dissociation on Fe(100). Initial state: (a) H_2S at the bridge site. Final states: (b) and (c) HS and H coadsorbed at neighboring hollow sites. Fe atoms are in gray, S atoms are in white, and H atoms are in black.

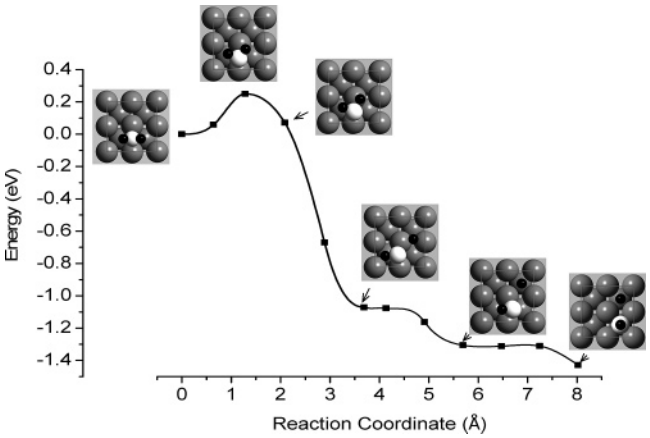

Figure 6. DFT-GGA(PBE) minimum energy path of H_2S dissociation on Fe(100) and several intermediate structures along the path.

requires that the initial and final states of the transition be known beforehand. We chose the most stable site as the initial state, the bridge site of H_2S on Fe(100) shown in Figure 5a. For the final state, we initially chose a configuration as in Figure 5b, because we know that both HS and H prefer the hollow site. We explored several paths from the initial state of Figure 5a to the final state of Figure 5b and found that all of the highest energy states along those paths are not true transition states, but higher-order saddle points. We then tried as the final state the configuration shown in Figure 5c. A preliminary run showed that a true transition state exists along this path. We then converged the MEP. Figure 6 shows the MEP with Figure 5a and c as the initial and final states, respectively. One can see that H_2S breaks one H−S bond by rotating one H atom toward a nearby surface Fe atom and the H−S bond dissociates over that Fe atom. The dissociation barrier is 0.25 eV, indicating the ease of breaking the H−S bond on Fe(100). At the transition state, the length of the breaking H−S bond is 1.378 Å, only 0.005 Å longer than the initial state, consistent with the expectation of an "early" transition state for a significantly exothermic reaction. After the transition state, one H atom breaks away and moves to the bridge site with a ~1.30 eV energy drop. The system then descends through two flat steps to reach the final state: the first step corresponds to diffusion of H from the bridge site to the hollow site (0.20 eV downhill); the second step corresponds to diffusion of HS from the bridge site to the hollow site (0.10 eV downhill).

5. HS Dissociation on Fe(100). In this investigation of how HS dissociates on Fe(100), we ignore the effect of the neighboring H atom (produced from H_2S dissociation) on the dissociation of HS, because, as we noted above, the diffusion barrier for H on Fe(100) is very low. Therefore, we expect H to diffuse away promptly. Because we find that both S and H prefer hollow sites, we choose a final state with S and H on neighboring hollow sites. Figure 7 shows the MEP for HS

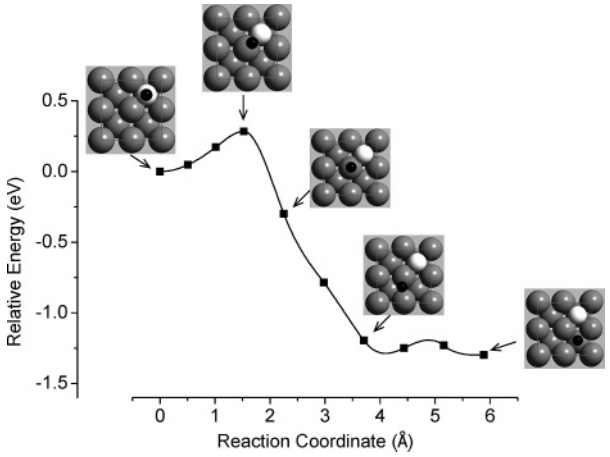

Figure 7. DFT-GGA(PBE) minimum energy path of HS dissociation on Fe(100) and several intermediate structures along the path.

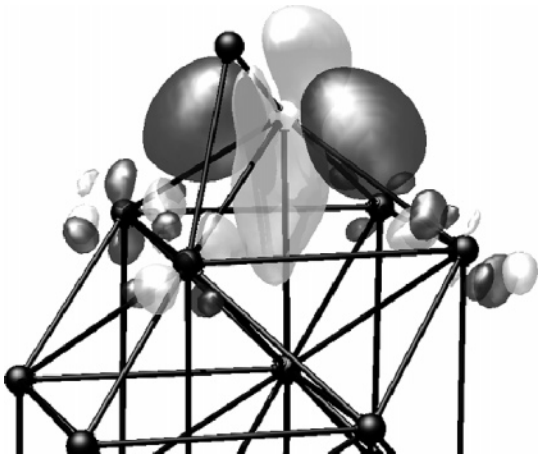

Figure 8. Isosurface plot of the electron density difference, $\Delta\rho$, for HS/Fe(100) in the transition state. Solid balls represent atoms: the top black one is H, S is in white, and the atoms below S are Fe atoms. The iso-value is at -0.05 e/Å^3 for the light gray surface and at 0.05 e/Å^3 for the dark gray surface. Negative $\Delta\rho$ indicates loss of electron density upon binding.

dissociation starting from the hollow site minimum. Like H_2S dissociation, HS breaks its H−S bond also by tilting the H atom toward a surface Fe atom. The barrier is 0.28 eV, similar to the magnitude of the barrier for the first H_2S dehydrogenation step. After the transition state, the H atom moves on top of a surface Fe atom and then on to a bridge site. The bridge site is an intermediate state for H in Figure 7. The second small barrier corresponds to the diffusion of H from the bridge site to the hollow site in the presence of S atom.

To gain more insight into the H−S bond-breaking process, we examine an electron density difference plot for the transition state of HS dissociation on Fe(100) in Figure 8. We see clearly that some electron density has moved away from the H−S bonding region. Moreover, electron density depletion is seen in the region between the S atom and the Fe(100) hollow site and the region above the S atom. Electron density accumulates mainly between S and Fe atoms on the flanks of the tilted HS group, indicating that the increased bonding between HS and Fe(100) is at the expense of the weakening of the HS bond. Some small amounts of electron density depletion and accumulation are also seen around all of the surface Fe atoms. Importantly, Figure 8 demonstrates that all surface Fe atoms coordinated around HS participate in the H−S bond breaking, despite the fact that Figure 7 shows that HS dissociates on top of a single Fe atom. Last, one might have expected HS to break by tilting the HS bond toward the bridge site. Just as we found for H_2S dissociation, the bridge-site path has a higher barrier and is also a higher-order saddle point.

In studying the hydrogenation of sulfur on Pt(111), as well as other reactions, Hu and co-workers proposed[34] a relationship between the structure of the transition state and the valency of a reactant. They suggested that divalent reactants such as O and S tend to have a transition state at the bridge site when they are hydrogenated. In particular, they found[35] that hydrogenation of S on Pt(111), that is, the reverse of HS dissociation, follows this rule. However, the above analysis demonstrates that the dissociation of HS on Fe(100) does not, indicating that this proposed transition state−valency relationship is not universally true.

Conclusions

Using periodic density functional theory within the generalized-gradient approximation to electron exchange and correlation, we have studied H_2S, HS, and S adsorption and diffusion, as well as H_2S and HS dissociation on Fe(100) at $\theta = 0.25$ ML. We find that H_2S is weakly molecularly adsorbed on a bridge site of Fe(100) with the molecular plane oriented along the surface normal. The adsorption of H_2S in a bridge site is exothermic by $\leq$0.46 eV. Adsorption at an on-top site is also a local minimum for H_2S on Fe(100), but this site is 0.13 eV less stable than the bridge site. The diffusion barrier from the bridge site to the on-top site is predicted to be $\sim$0.15 eV. In contrast to H_2S, HS is strongly chemisorbed on Fe(100). The only stable configuration of HS on Fe(100) has S in the hollow site and the HS bond upright, to engage favorably the S p-orbitals in Fe−S bonding, with a predicted binding energy of 3.56 eV. Last, we find that S atom strongly binds to the hollow site of Fe(100). The bridge site serves as a transition state for diffusion between two neighboring hollow sites for S/Fe(100) and HS/Fe(100).

With the climbing-image nudged elastic band method, we have obtained the minimum energy path for H_2S and HS dehydrogenation on Fe(100). Starting from the bridge site, we predict that H_2S loses one H atom by rotating the molecule to orient the H atom toward one of the Fe atoms coordinated to the S atom. The dissociation barrier is very small, 0.25 eV. Beginning with hollow site adsorption, HS breaks its bond also by tilting the H atom toward a nearby Fe atom. The H−S bond breaks on top of the Fe atom, with a barrier of 0.28 eV. These low barriers are consistent with the observed dissociation of H_2S above 190 K. Although both H_2S and HS dehydrogenation processes break the H−S bond on top of one Fe atom, charge density difference plots indicate that all surface Fe atoms coordinated to S participate in the dissociation process. These predictions could be verified by low-temperature scanning tunneling microscopy, which recently captured single-molecule events of H_2S dissociation on the Cu(100) surface.[30]

Acknowledgment. This work was supported by the Army Research Office. We thank the Maui High Performance Computing Center and the NAVO Major Shared Resources Center for CPU time.

References and Notes

(1) Woods, T. L. *Thermodynamic Values at Low Temperature for Natural Inorganic Materials: an uncritical summary*; Oxford University Press: New York, 1987.

(2) Hegde, R. I.; White, J. M. *J. Phys. Chem.* **1986**, *90*, 296.

(3) Huntley, D. R. *Surf. Sci.* **1990**, *240*, 13.

(4) Blyth, R. I. R.; Searle, C.; Tucker, N.; White, R. G.; Johal, T. K.; Thompson, J.; Barrett, S. D. *Phys. Rev. B* **2003**, *68*, 205404.
(5) Cote, P. J.; Rickard, C. *Wear* **2000**, *241*, 17.
(6) Rice, J. R.; Wang, J. S. *Mater. Sci. Eng., A* **1989**, *107*, 23.
(7) Srikrishnan, V.; Liu, H. W.; Ficalora, P. J. *Scr. Metall.* **1975**, *9*, 1341.
(8) Briant, C. L.; Sieradzki, K. *Phys. Rev. Lett.* **1989**, *63*, 2156.
(9) Narayan, P. B. V.; Anderegg, J. W.; Chen, C. W. *J. Electron Spectrosc. Relat. Phenom.* **1982**, *27*, 233.
(10) Baer, D. R.; Thomas, M. T.; Jones, R. H. *Metall. Mater. Trans. A: Phys. Metall. Mater. Sci.* **1984**, *15A*, 853.
(11) Shanabarger, M. R.; Moorhead, R. D. *Surf. Sci.* **1996**, *365*, 614.
(12) Cabibil, H.; Kelber, J. A. *Surf. Sci.* **1997**, *373*, 257.
(13) Hohenberg, P.; Kohn, W. *Phys. Rev.* **1964**, *136*, B864.
(14) Kohn, W.; Sham, L. J. *Phys. Rev.* **1965**, *140*, A1133.
(15) Kresse, G.; Furthmüller, J. *Phys. Rev. B* **1996**, *54*, 11169.
(16) Kresse, G.; Furthmüller, J. *Comput. Mater. Sci.* **1996**, *6*, 15.
(17) Blöchl, P. E. *Phys. Rev. B* **1994**, *50*, 17953.
(18) Kresse, G.; Joubert, D. *Phys. Rev. B* **1999**, *59*, 1758.
(19) Perdew, J. P.; Burke, K.; Ernzerhof, M. *Phys. Rev. Lett.* **1996**, *77*, 3865.
(20) Monkhorst, H. J.; Pack, J. D. *Phys. Rev. B* **1976**, *13*, 5188.
(21) Methfessel, M.; Paxton, A. T. *Phys. Rev. B* **1989**, *40*, 3616.
(22) Jiang, D. E.; Carter, E. A. *Phys. Rev. B* **2003**, *67*, 214103.
(23) Acet, M.; Zähres, H.; Wassermann, E. F.; Pepperhoff, W. *Phys. Rev. B* **1994**, *49*, 6012.
(24) Jónsson, H.; Mills, G.; Jacobsen, K. W. Classical and Quantum Dynamics in Condensed Phase Simulations. In *Classical and Quantum Dynamics in Condensed Phase Simulations*; Berne, B. J., Ciccotti, G., Coker, D. F., Eds.; World Scientific: Singapore, 1998; p 385.
(25) Henkelman, G.; Uberuaga, B. P.; Jónsson, H. *J. Chem. Phys.* **2000**, *113*, 9901.
(26) Watanabe, M. *Nippon Kagaku Kaishi* **1977**, 1762.
(27) Weir, T.; Simmons, G. W. *AIP Conf. Proc.* **1982**, *84*, 113.
(28) Hammer, B.; Hansen, L. B.; Nørskov, J. K. *Phys. Rev. B* **1999**, *59*, 7413.
(29) Dion, M.; Rydberg, H.; Schroeder, E.; Langreth, D. C.; Lundqvist, B. I. *Phys. Rev. Lett.* **2004**, *92*, 246401.
(30) Lauhon, L. J.; Ho, W. *J. Phys. Chem. B* **2001**, *105*, 3987.
(31) Legg, K. O.; Jona, F.; Jepsen, D. W.; Marcus, P. M. *Surf. Sci.* **1977**, *66*, 25.
(32) Chubb, S. R.; Pickett, W. E. *Phys. Rev. B* **1988**, *38*, 12700.
(33) Jiang, D. E.; Carter, E. A. *Phys. Rev. B* **2004**, *70*, 064102.
(34) Michaelides, A.; Hu, P. *J. Am. Chem. Soc.* **2000**, *122*, 9866.
(35) Michaelides, A.; Hu, P. *J. Chem. Phys.* **2001**, *115*, 8570.
(36) Herzberg, G. *Molecular Spectra and Molecular Structure, 3: Electronic Spectra and Electronic Structure of Polyatomic Molecules*; Krieger Pubishing Co.: Malabar, FL, 1966.
(37) Shiell, R. C.; Hu, X. K.; Hu, Q. J.; Hepburn, J. W. *J. Phys. Chem. A* **2000**, *104*, 4339.
(38) Huber, K. P.; Herzberg, G. *Molecular Spectra and Molecular Structure, 4: Constants of Diatomic Molecules*; Van Norstrand Reinhold Co.: New York, 1979.
(39) Sorescu, D. C.; Thompson, D. L.; Hurley, M. M.; Chabalowski, C. F. *Phys. Rev. B* **2002**, *66*, 035416.
(40) Eder, M.; Terakura, K.; Hafner, J. *Phys. Rev. B* **2001**, *6411*, 115426.
(41) Nayak, S. K.; Nooijen, M.; Bernasek, S. L.; Blaha, P. *J. Phys. Chem. B* **2001**, *105*, 164.
(42) Wang, Z. Q.; Li, Y. S.; Jona, F.; Marcus, P. M. *Solid State Commun.* **1987**, *61*, 623.